9372 *Biochemistry* **2009,** *48,* 9372–9383
DOI: 10.1021/bi901222p

BIOCHEMISTRY
including biophysical chemistry & molecular biology
Article

Comparative Study of Two Plasticins: Specificity, Interfacial Behavior, and Bactericidal Activity[†]

Pierre Joanne,[‡] Mélanie Falord,[§] Olivier Chesneau,[∥] Claire Lacombe,[‡,○] Sabine Castano,[⊥] Bernard Desbat,[⊥] Constance Auvynet,[@] Pierre Nicolas,[‡] Tarek Msadek,[§] and Chahrazade El Amri*[,‡,#]

[‡]*Université Pierre et Marie Curie, ER3-Biogénèse des signaux peptidiques, 7 quai St Bernard, 75251 Paris Cedex 05, France,* [§]*Institut Pasteur, Biology of Gram Positive Pathogens, CNRS URA 2172 25, Rue du Dr Roux, 75724 Paris Cedex 15, France,* [∥]*Institut Pasteur, Unité des Membranes Bactériennes, CNRS URA 2172 25, Rue du Dr Roux, 75724 Paris Cedex 15, France,* [⊥]*Université Bordeaux I, ENITAB, CBMN, UMR5248, CNRS, 2, rue Robert Escarpit, 33607 Pessac, France, and* [@]*Universidad Nacional Autónoma de México, Departamento de Medicina Molecular y Bioprocesos, Instituto de Biotecnologia, Avenida Universidad 2001, Col Chamilpa, Cuernavaca, Mor. 62270, Mexico.* [○]*Present address: UMR 7203-Laboratoire des Biomolécules, Structure et Fonction des Molécules Bioactives, 4 Place Jussieu, 75252 Paris Cedex 05, France.* [#]*Present address: Université Pierre et Marie Curie, UR4-Enzymologie Moléculaire et Fonctionnelle, 7 quai St Bernard, 75252 Paris Cedex 05, France.*

Received July 17, 2009; Revised Manuscript Received August 25, 2009

ABSTRACT: A comparative study was designed to evaluate the staphylococcidal efficiency of two sequence-related plasticins from the dermaseptin superfamily we screened previously. Their bactericidal activities against *Staphylococcus aureus* as well as their chemotactic potential were investigated. The impact of the GraS/GraR two-component system involved in regulating resistance to cationic antimicrobial peptides (CAMPs) was evaluated. Membrane disturbing activity was quantified by membrane depolarization assays using the diS-C3 probe and by membrane integrity assays measuring β-galactosidase activity with recombinant strain ST1065 reflecting compromised membranes and cytoplasmic leakage. Interactions of plasticins with membrane models composed of either zwitterionic lipids mimicking the *S. aureus* membrane of CAMP-resistant strains or anionic lipids mimicking the negative charge-depleted membrane of CAMP-sensitive strains were analyzed by jointed Brewster angle microscopy (BAM), polarization modulation infrared reflection absorption spectroscopy (PM-IRRAS), and differential scanning calorimetry (DSC) to yield detailed information about the macroscopic interfacial organization, in situ conformation, orientation of the peptides at the lipid−solvent interface, and lipid-phase disturbance. We clearly found evidence of distinct interfacial behaviors of plasticins we linked to the distribution of charges along the peptides and structural interconversion properties at the membrane interface. Our results also suggest that amidation might play a key role in GraS/GraR-mediated CAMP sensing at the bacterial surface.

Many species, from bacteria to humans, produce antimicrobial peptides (AMPs)[1] whose role is to defend organisms against infections. These peptides are active against a broad spectrum of bacteria, fungi, yeast, and protozoa (*1*, *2*). In higher organisms, they are synthesized by epithelial cells and circulating leukocytes and, in general, are cationic and amphipathic (*3*). Because of their electrostatic properties, cationic AMPs (CAMPs) can easily bind to the negatively charged bacterial cell envelope and inactivate bacteria, e.g., by forming pores in the bacterial membrane leading to bacterial lysis (*4*). Their original mode of action allows them to lower the risk of microbial resistance (*1*, *5*). The current increase in the levels of bacterial resistance makes it necessary to identify and develop novel antimicrobial agents. Methicillin-resistant *Staphylococcus aureus* (MRSA) strains have emerged as superbug pathogens, both in hospital settings and in the community (*6*, *7*). In this respect, CAMPs are of interest as alternative therapeutics or as adjuvants to staphylococcidal compounds (*8*). However, they need to be rationally optimized by structural and functional studies.

Gram-positive pathogens such as *S. aureus* resist the action of some CAMPs by increasing their cell-surface positive charges, both through D-alanylation of wall teichoic acids and phospholipid lysylination, leading to electrostatic repulsion of CAMPs (*9*). The *dltABCD* and *mprF* genes encoding the enzymes involved in these two mechanisms, respectively, are known to be positively controlled by a two-component system (TCS) designated GraS/GraR or ApsS/ApsR (*10*, *11*). TCSs are bacterial signal transduction

[†]This work was supported by the University Pierre et Marie Curie (Paris 6), CNRS, and the Association Nationale pour la Recherche (ANR-Prob DOM). Work in the group of T.M. was supported by research funds from the European Commission (Grants BaSysBio, LSHG-CT-2006−037469, and StaphDynamics, LHSM-CT-2006-019064), the Centre National de la Recherche Scientifique (CNRS URA 2172), and the Institut Pasteur.

*To whom correspondence should be addressed: Université Pierre et Marie Curie, UR4-Enzymologie Moléculaire et Fonctionnelle, 7 quai St Bernard, 75252 Paris Cedex 05, France. Telephone: + 33 (1) 44 27 69 52. Fax: + 33 (1) 44 27 51 40. E-mail: chahrazade.el_amri@upmc.fr.

[1]Abbreviations: AMPs, antimicrobial peptides; ATR-FTIR, attenuated total reflectance FTIR; BAM, Brewster angle microscopy; BHI, brain−heart infusion; BSA, bovine serum albumin; CAMPs, cationic antimicrobial peptides; diS-C_3(5), 3,3′-dipropylthiadicarbocyanine; DMPC, 1,2-dimyristoyl-*sn*-glycero-3-phosphatidylcholine; DMPE, 1,2-dimyristoyl-*sn*-glycero-3-phosphoethanolamine; DMPG, 1,2-dimyristoyl-*sn*-glycero-3-phosphatidylglycerol; DSC, differential scanning calorimetry; fMLP, formyl methionyl-leucyl-phenylalanine; FTIR, Fourier transform infrared; HK, histidine kinase; LUVs, large unilamellar vesicles; MLVs, multilamellar vesicles; MIC, minimal inhibitory concentration; MRSA, methicillin-resistant *Staphylococcus aureus*; PBS, phosphate-buffered saline; PE, phosphatidylethanolamine; PG, phosphatidylglycerol; PM-IRRAS, polarization modulation infrared reflection absorption spectroscopy; ONPG, *o*-nitrophenyl β-galactoside; ONP, *o*-nitrophenol; RPMI, Roswell Park Memorial Institute; RR, response regulator; TCS, two-component system; TSB, tryptic soy broth.

 Published on Web 08/27/2009

Table 1: Amino Acid Sequences and Physicochemical Characteristics of Investigated Plasticins[a]

Peptide	Sequence	Net Charge	Mean Hydrophobicity	Mean Hydrophobic Moment (μH)
Plasticin-B1[b] (DRP-PBN2)	GLVTSLIKGAGKLLGGLFGSVTGGQS	+2	0.33	3.0
[$K^{8,12}$, F^{18}]-Plasticin-DA1[b] (DRP-PD36KF)	GVVTDLLKTAGKLLGNLFGSLSG-NH2	+2	0.5	3.96
Plasticin-B1a[b] (DRP-PBN2a)	GLVTSLIKGAGKLLGGLFGSVTG-NH2	+3	0.92	3.42
Plasticin-DA1[b] (DRP-PD 3-6)	GVVTDLLNTAGGLLGNLVGSLSG-NH2	0	0.7	3.44

[a]Amino acid sequences, net charges, mean hydrophobicities, and mean hydrophobic moments (using the CSS scale) were calculated using HydroMCalc (http://www.bbcm.univ.trieste.it/~tossi/HydroCalc/HydroMCalc.html). The net charge of the plasticins is given for pH 7. [b]Names of plasticins are indicated according to the new proposed nomenclature (*55*). Ancient names are given in parentheses.

pathways with a sensor histidine kinase (HK) that is autophosphorylated in response to specific environmental stimuli; the transfer of the phosphoryl group to its cognate response regulator (RR) acts to regulate target gene expression. The GraS HK is specifically involved in CAMP sensing, promoting bacterial resistance through its RR GraR (*10*). However, only a few studies have been reported on the effect of the two-component system, in both Gram-negative (PhoPQ) and Gram-positive (GraS/GraR) bacteria, on the antimicrobial activity of AMPs. A better understanding of the mechanisms of action of CAMPs against sensitive and resistant cells is essential to the development of models that will be used as the basis for new drug design (*12*). Furthermore, CAMPs also induce several immunomodulating functions, such as chemotaxis through cell surface receptors (*13*, *14*). Given the primary role of neutrophils in innate immunity defense mechanisms against *S. aureus* provided by neutrophils (*15*), topical applications of immunostimulating CAMPs could be highly desirable in combating staphylococcal infections (*16*).

AMPs of the plasticin family belong to the dermaseptin family of host defense peptides produced by the skin of hylid frogs (*1*, *3*, *17*). Plasticins are rich in Gly and Leu residues arranged in regular 5-mer motifs, GXXXG (where X is any amino acid residue), have very similar amino acid sequences, hydrophobicities, and amphipathicities, but differ markedly in their net charge, conformational plasticity, and activity spectra (Table 1) (*3*). In previous studies, different plasticin parameters, including effects of charge, hydrophobicity, degree of structure formation, amphipathicity, size of the polar and apolar sectors, and structural flexibility, were analyzed (*18*−*20*). Differences in their membrane adsorption capacity, antibacterial potency, and capacities to disturb and reorganize membrane lipids in relation with their chameleon-like character were highlighted (*19*, *21*).

In this study, the capacity of plasticins to inhibit growth of various *S. aureus* strains as well as the role the GraS/GraR TCS plays in controlling resistance to plasticins was investigated. In addition, their chemotactic potential was compared. We measured in vivo the impact of plasticins on *S. aureus* resistant and nonresistant strains through membrane depolarization and membrane permeabilization assays. Wimley and co-workers have emphasized the importance of interfacial activity, i.e., the capacity to destabilize membranes by partitioning into membrane interfaces, disturbing the organization of lipids independently from peptide conformation, and hence breaking down the permeability barrier (*22*, *23*). By using model membranes mimicking the cytoplasmic membrane of *S. aureus* resistant and sensitive strains, we evaluated the affinity of plasticins for the interface and examined macroscopic interfacial organization by Brewster angle microscopy (BAM). In situ conformations, orientations at the lipid−solvent interface, and phospholipid perturbations were determined by polarization modulation infrared reflection absorption spectroscopy (PM-IRRAS). Differential scanning calorimetry studies were also undertaken to study the effect of selected plasticins on lipid-phase transitions. We show here that structural interconversions at the membrane interface of the representative plasticins rather than their secondary structures provide clues explaining differences in their efficacy toward *S. aureus*.

MATERIALS AND METHODS

Materials. Synthesis and purification of plasticins (Table 1) were performed by the Plateforme Ingénierie des Protéines et Synthèse Peptidique of IFR 83 (Université Pierre et Marie Curie, Paris, France). They were purified using reverse-phase high-performance liquid chromatography (RP-HPLC) on a semipreparative C18 column, and mass spectrometry was used to confirm purity. Lipids were purchased from Genzyme pharmaceuticals. Organic solvents and salts were from Sigma (Saint-Quentin Fallavier, France). Media for cell culture were from Invitrogen (Cergy-Pontoise, France) and those for bacteria from Oxoid (Basingstoke, U.K.). Ultrapure water (Milli-Q, Millipore) was used for all experiments.

Bacterial Strains. *S. aureus* strain RN1 HG is a *rsbU*+ derivative of strain NCTC 8325 (S. Herbert and F. Götz, University of Tübingen, Tübingen, Germany, unpublished observations). *S. aureus* strain ST1036 is a Δ*graRS* mutant derivative of strain RN1 HG, constructed using the pMAD vector (*24*) via removal of the entire TCS coding sequence (M. Falord, unpublished observations). Plasmid pSA14 (M. Débarbouillé, unpublished results) was used to construct a transcriptional *lacZ* reporter fusion. Plasmid pSA14 was constructed by cloning a 3.2 kb *Eco*RI−*Pst*I DNA fragment from plasmid pHT304-18Z (*25*) between the corresponding restriction sites of the pMK4 shuttle vector (*26*). The insert carried the promoterless

Table 2: MIC Values of Plasticins toward *S. aureus*[a]

microorganism	plasticin-B1	[$K^{8,12}$,F^{18}]plasticin-DA1	plasticin-B1a
S. aureus RN4220 with msr(A) (*32*)	50	> 50	25
S. aureus SK982 with qacA (*56*)	50	> 50	12.5
S. aureus MW2[b] (*6*)	25	> 50	12.5
S. aureus N315[b] (*57*)	12.5	> 50	12.5
S. aureus COL[b] (*7*)	50	> 50	12.5
S. aureus BM12623[b] (*37*)	25	> 50	12.5

[a]Values are expressed in micromolar. Strains were representatives of various *S. aureus* lineages. The neutral plasticin-DA1 was also investigated but found to be inactive (data not shown). [b]Clinical multi-drug-resistant isolates.

Escherichia coli lacZ gene downstream from the *Bacillus subtilis spoVG* ribosome binding site (*27*, *28*). The *tufA* gene promoter was amplified from the pCtuf*gfp* vector (*29*) using *Pwo* thermostable DNA polymerase (Roche) and oligodeoxynucleotides MF97 (5′ CTGCTGCAGTCGTTCGGTTATGCAA 3′) and MF98 (5′ GGAGGATCCACTCTCTCATGATAGTTTCT 3′). The corresponding 324 bp promoter fragment was then cloned between the *Pst*I and *Bam*HI restriction sites of the pSA14 vector, giving plasmid pSAtuf*lacZ*, which was introduced into *S. aureus* strain RN4220 resulting in strain ST1065. Strong and stable β-galactosidase activity was measured for this strain, making it highly useful for membrane permeabilization assays, through detection of cytoplasmic enzyme activity leakage.

Chemotaxis Assay. Polynuclear neutrophils were isolated from heparinized peripheral blood from healthy adult donors using dextran sedimentation, Ficoll-Hypaque gradient centrifugation, and hypotonic lysis (*30*). Cells were washed and resuspended in chemotaxis medium (RPMI 1640, 1% BSA). Chemotaxis assays on neutrophils were performed using a 48-well microchemotaxis chamber (Neuro Probe) as described previously (*31*). Briefly, different concentrations of plasticin-B1 or [$K^{8,12}$,F^{18}]plasticin-DA1 in chemotaxis medium (RPMI 1640, 1% BSA) were placed in the bottom wells of the chamber. Prior to migration assays, neutrophils were loaded for 30 min with 10 μg/mL calcein (AM, Molecular Probes) and cell migration was assessed by measuring the fluorescence of the lower face of the separating membrane with an Alpha Innotech image analyzer, using Fluorchem 8800 from Alpha Innotech. fMLP (formyl methionyl-leucyl-phenylalanine) was used as a positive control and medium as a negative control.

Growth Inhibition Assays. *S. aureus* strains (Table 2) were grown overnight as described previously (*32*). Minimum inhibitory concentrations (MIC) of peptides were determined in duplicate by the agar-dilution method after incubation for 16 h at 37 °C. For each strain, a 10 μL inoculum of a 0.5× McFarland suspension was spotted on Mueller Hinton agar plates with 2-fold serial dilutions of the tested peptides.

Bactericidal Assays. Bactericidal effects of the two staphylocidal active plasticins, carboxamidated plasticin-B1 and [$K^{8,12}$, F^{18}]plasticin-DA1, against the *S. aureus* RN1 HG virulent strain were compared. An overnight culture was diluted in TSB (tryptic soy broth) medium to an absorbance (A_{600}) of 0.03 and grown at 37 °C to an A_{600} of 1. The culture was split into three, and either sterile water (control) or each of the two peptides was added at a final concentration of 200 μM. CFU (colony forming units) counts were performed on cultures before peptide addition and after incubation for 5, 15, and 30 min at 37 °C. Samples were appropriately diluted in TSB, spread onto TSA plates, and incubated at 37 °C. The number of CFU per milliliter was determined after incubation for 24 h. The experiment was performed in duplicate.

Microwell Cultures with and without Plasticins. *S. aureus* RN1 HG and ST1036 (Δ*graRS*) were grown overnight in TSB medium at 37 °C and then diluted to an A_{600} of 0.05 in TSB. Dilutions of plasticin-B1a and [$K^{8,12}$,F^{18}]plasticin-DA1 were created at 2-fold final concentrations, and 50 μL of each were then added to 50 μL of diluted cultures in a 96-well microtiter plate. Wells containing TSB alone or with different amounts of peptides and TSB with diluted cultures with no added peptides were included as controls. Plates were incubated for 15 h with vigorous shaking at 37 °C in a Synergy 2 multi-detection microplate reader (BioTek Instruments Inc., Winooski, VT), and A_{600} was measured every 20 min. Tests were performed in triplicate.

Membrane Depolarization Assay. The effect of the peptides on membrane potential was tested using the fluorescent membrane potential-sensitive probe 3,3′-dipropylthiadicarbocyanine iodide [diS-C_3(5)] (Molecular Probes-Invitrogen) (*33*). *S. aureus* ST1065 was grown at 37 °C to midlogarithmic phase, washed twice in HEPES buffer [5 mM HEPES and 5 mM glucose (pH 7.2)], and suspended in the same buffer at an A_{600} of 0.2. Fluorescence emission was monitored at 37 °C using a Perkin-Elmer LS 50B spectrofluorometer with Spectro Winlab software at 670 nm (excitation at 622 nm). After temperature equilibration, 1 μM diS-C_3(5) was added to the cell suspension. The probe concentration used in the assay was not toxic for the strain. Once the dye uptake was maximal as indicated by a stable reduction in fluorescence due to quenching of the accumulated dye in the bacteria, 0.1 M KCl was added to maintain a high membrane potential gradient (*34*). Then the desired concentration (10−50 μM) of test peptide was added. Finally, the membrane potential was fully dissipated with Triton X-100 (final concentration of 0.1%). The membrane potential dissipating activity (Da) of the peptides is expressed as a percentage using the following formula:

$$\mathrm{Da} = \frac{F_\mathrm{p} - F_0}{F_\mathrm{T} - F_0} \times 100$$

In HEPES-glucose, F_0 is the stable fluorescence after addition of KCl, F_P is the fluorescence 10 min after addition of peptide, and F_T is the fluorescence after addition of Triton.

Membrane Permeabilization Assay. *S. aureus* strain ST1065 was used to test the membrane permeabilization potential of selected plasticins. Permeabilization of the cytoplasmic membrane of *S. aureus* ST1065 was assayed by measuring β-galactosidase activity with the chromogenic substrate ONPG. Bacteria were grown in 10% Luria-Bertani broth (LB), washed twice with PBS [0.15 M phosphate and 0.2 M NaCl (pH 7.4)], and diluted to an A_{630} of 0.5 in 10% LB in PBS. The assay was

conducted in a 96-well microtiter plate. Aliquots (15 μL) of bacterial suspensions were mixed with 2.5 mM ONPG and incubated with various concentrations of peptide in a final volume of 150 μL. ONPG hydrolysis was monitored by measuring the A_{405} of released *o*-nitrophenol with a FluostarGalaxy microtiter plate reader (BMG LabTech). Each assay was repeated three times, and a representative curve is shown.

Surface Pressure and Brewster Angle Microscopy (BAM) Measurements. Experiments were performed on a computer-controlled Langmuir film balance (Nima Technology, Coventry, England). The rectangular trough (V = 75 mL, S = 95 cm^2) and the barrier were made of Teflon. The trough was filled with a phosphate-buffered saline (PBS) solution [100 mM phosphate and 150 mM NaCl (pH 7.0)]. The experiments were conducted at room temperature. After deposition (or not) of a small quantity of DMPC (in pure chloroform) or DMPG [in chloroform and methanol (1:1, v/v)] at the air−water interface of the buffer solution and compression of the monolayer thus formed at 25 mN/m, a few microliters (to reach a concentration of 0.1 μM) of each peptide was injected into the subphase. Surface pressure variation (Π) was measured by the Wilhelmy method using a Whatman filter paper plate. The morphology of the interface was observed with a Brewster angle microscope (NFT BAM*2plus*, Göttingen, Germany) mounted on the Langmuir trough. The microscope was equipped with a frequency-doubled Nd:Yag laser (532 nm, 55 mW), a polarizer, an analyzer, and a CCD camera. The spatial resolution of the BAM was ~2 μm, with a 650 μm × 450 μm image size and a 10× lens. The BAM images are coded in gray level, which can be calibrated in absolute reflectance. The calibration function is established by comparison between the experimental curve of the gray level and the theoretical Fresnel curve on the water surface. Thickness was evaluated by the proportional relationship between the reflectance of the film and the square of its interfacial thickness when its optical index is assumed to be constant, displayed as different gray levels (*35*).

PM-IRRAS. PM-IRRAS spectra were recorded on a Nicolet Nexus 870 spectrometer equipped with a photovoltaic HgCdTe detector cooled to 77 K. This device was mounted on the Langmuir trough described above. The same method of lipid deposition and peptide injection as in the BAM experiments was applied, and 600 scans at a resolution of 8 cm^{-1} were gathered. Treatment of spectra and decomposition of the amide I and amide II spectral region were performed as previously described (*36*).

Differential Scanning Calorimetry (DSC). One milligram of DMPC or DMPG was dissolved with 100 μL of chloroform or 100 μL of a chloroform/methanol mixture (1:1, v/v), respectively. Lipid films were obtained by evaporation of solvents under a nitrogen stream. The films thus obtained were desiccated for several hours under vacuum at 40 °C. Lipids were then suspended in PBS [100 mM phosphate and 150 mM NaCl (pH 7.0)] to yield multilamellar vesicles (MLVs) at a final concentration of 1 mg/mL. Peptides were added to the PBS solution at a concentration that allows a lipid:peptide ratio of 100:1, 50:1, or 20:1. This solution and 1 mL of PBS were then degassed under vacuum for 15 min. The PBS solution was then loaded into the reference cell of the Nano-Differential Scanning Calorimeter III (Calorimetry Sciences Corp., Lindon, Utah), and the lipid/peptide solution was loaded into the sample cell. Scans were recorded between 0 and 40 °C at a scan rate of 0.5 °C/min for heating and 1 °C/min for cooling. Thermogram analyses were performed with CpCalc, the software provided with the calorimeter. Final figures were plotted with Origin 6 (Microcal, Inc.).

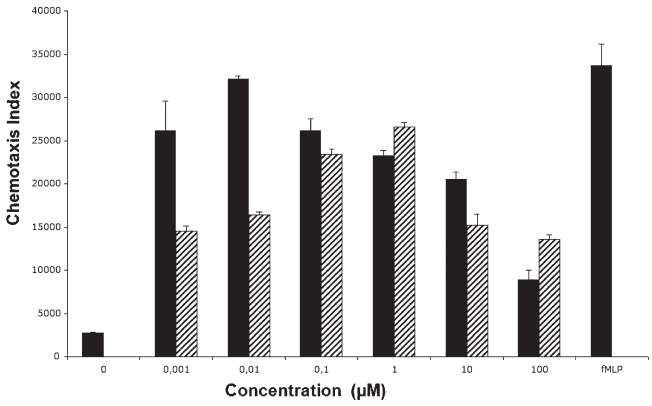

FIGURE 1: Chemotactic activities of plasticins. Neutrophil migration induced by plasticin-B1 (black bars) or [K^{8,12},F^{18}]plasticin-DA1 (hatched bars) at 37 °C using fMLP as a positive control and culture medium as a negative control.

RESULTS

Plasticin B1 and [K^{8,12},F^{18}]plasticin-DA1 share 61.5% amino acid identity. It is worth mentioning that the 10 nonidentical amino acids have, in general, similar polarities (Table 1). The two peptides bear the same net charge (+2), but their charge distribution is different. Indeed, plasticin-B1 contains two positively charged lysine residues, whereas an additional aspartate residue in position 5 together with a C-terminal amidation generates a peptide with an equivalent net charge for [K^{8,12}, F^{18}]plasticin-DA1. The two peptides have identical overall hydrophobicities and amphipathicities, corresponding to a hydrophobic sector that subtends a radial angle of 180° on a helical wheel projection (Table 1 and ref *17*). Glycine residues are predominant within the polar surface of the helix of both molecules, while leucine is predominant on the nonpolar surface. The carboxamidated version of plasticin-B1 and the neutral parent of [K^{8,12},F^{18}]plasticin-DA1, plasticin-DA1, were used for comparison in some experiments.

Chemotactic Activities of Plasticins. Immunostimulatory properties are highly desirable when antibacterial compounds are being selected. We thus evaluated the capacity of plasticin-B1 and [K^{8,12},F^{18}]plasticin-DA1 to induce migration of human peripheral blood polynuclear neutrophils (Figure 1). For this cell type, the maximal response was observed for a concentration of 10 nM for plasticin-B1 while it was found to be 1 μM for [K^{8,12}, F^{18}]plasticin-DA1.

Activities of Plasticins against Various S. aureus Strains. We determined the MIC values of plasticins against different *S. aureus* strains, including multi-drug-resistant clinical isolates that are disseminated worldwide (Table 2). Interestingly, while plasticin-B1 and its carboxamidated version (plasticin-B1a) exhibited significant activity, [K^{8,12},F^{18}]plasticin-DA1 had no activity against multi-drug-resistant strains. More specifically, plasticin-B1a had a MIC in the range of 12.5 μM and plasticin-B1 had a MIC in the range of 25−50 μM. Plasticin-DA1, the neutral parent of [K^{8,12},F^{18}]plasticin-DA1, had no detectable activity against the strains employed in this study. These distinct antibacterial efficiencies were also observed for multi-drug-resistant *Staphylococcus epidermidis* and *Staphylococcus hemolyticus* strains (*37*) (Table S1 of the Supporting Information).

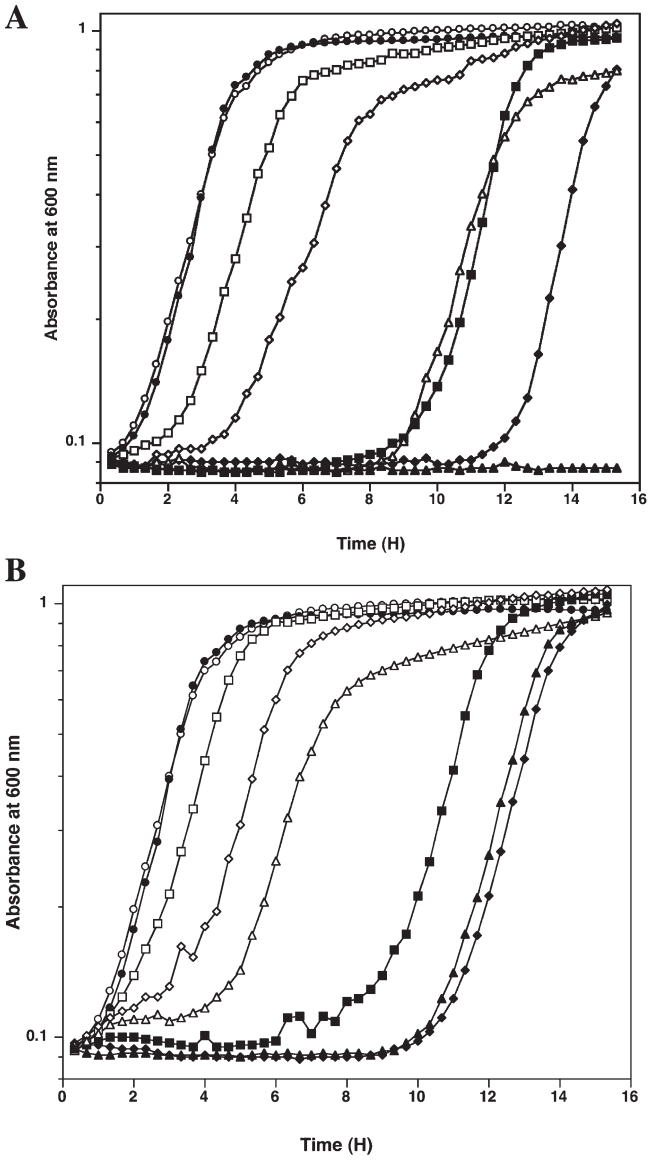

FIGURE 2: Effect of plasticins on the growth of *S. aureus* strains RN1 HG (empty symbols) and ST1036 Δ*graRS* (filled symbols). Strains were grown at 37 °C in TSB with plasticin-B1a (A) or [$K^{8,12}$,F^{18}]plasticin-DA1 (B) at 0 (○), 20 (□), 30 (◇), and 60 μM (△), and growth was followed by measuring absorbance at 600 nm using a microtiter plate reader. Each experiment was repeated three times, and a representative curve is shown.

Activities of Plasticins against S. aureus RN1 HG and ST1036 (Δ*graRS*). Since the GraS/GraR TCS is known to induce CAMP resistance in *S. aureus* (*10*), we investigated whether this resistance mechanism was also active against the plasticins. *S. aureus* RN1 HG and ST1036 (Δ*graRS*) growth in TSB was followed using a Biotek Synergy Microplate reader, with increasing concentrations of peptides. No significant growth differences were observed for the two strains without peptides, or in the presence of 100 μM plasticin-B1 (data not shown). However, the addition of plasticin-B1a or [$K^{8,12}$,F^{18}]plasticin-DA1 led to prolonged lag phases before growth resumed, in a dose-dependent manner, as shown in Figure 2. Interestingly, plasticin-B1a (Figure 2A) exhibited a stronger effect than [$K^{8,12}$,F^{18}]plasticin-DA1 (Figure 2B) toward the two strains since the lag phase of the parental RN1 HG strain ranged from approximately 30 min [20 μM (□)] to 9 h [60 μM (△)] with this peptide, whereas it did not exceed 4 h with up to 60 μM [$K^{8,12}$,F^{18}]plasticin-DA1.

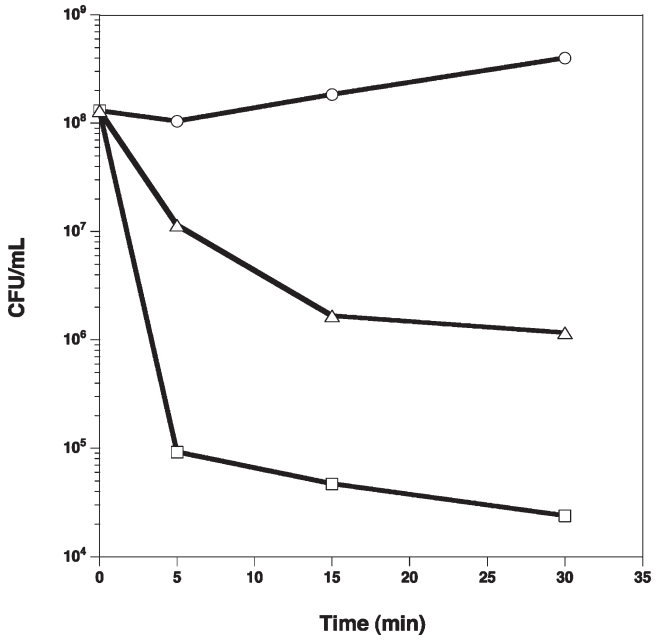

FIGURE 3: Bactericidal effects of plasticins on *S. aureus* RN1 HG. The strain was grown in TSB until the OD_{600} reached 1 and split into three cultures, with either plasticin-B1a (□) or [$K^{8,12}$,F^{18}]plasticin-DA1 (△) added at a final concentration of 200 μM or sterile water as a control (○). Killing was followed over a 30 min time period by determining the number of CFU per milliliter.

Moreover, the Δ*graRS* mutant always had a greater lag phase than the wild type at a defined concentration for both of the plasticins. While slight growth differences were observed for strain ST1036 (Δ*graRS*) with the two peptides at 10 μM (●), a strong bacteriostatic effect was visible beginning at 20 μM leading to complete growth inhibition of the Δ*graRS* mutant in the presence of plasticin-B1a at 60 μM [Figure 2A (▲)]. Unexpectedly, [$K^{8,12}$,F^{18}]plasticin-DA1 did not lead to complete growth arrest of the Δ*graRS* mutant even at 150 μM, with a 13 h lag phase instead (data not shown). Thus, two of the three tested plasticins exhibited a strong effect on *S. aureus* RN1 HG growth, with a stronger effect seen for plasticin-B1a, as well as an acute antimicrobial activity against the strain that lacks the *graRS* genes.

Bactericidal Effect of Plasticin on S. aureus RN1 HG. To compare the bactericidal effects of the two most active plasticins, *S. aureus* RN1 HG was grown in TSB until the OD_{600} reached 1. Plasticin-B1a or [$K^{8,12}$,F^{18}]plasticin-DA1 was then added at a final concentration of 200 μM, and bacterial viability was measured by determining the number of CFU over a 30 min incubation period, in comparison to a control culture to which only sterile water was added. As shown in Figure 3, both peptides had a dramatic effect on cell viability, with the loss of more than 99% of the viable cells after incubation for only 5 min. Plasticin-B1a was 40-fold more active than [$K^{8,12}$,F^{18}]plasticin-DA1, with only 0.02% viable cells after incubation for 30 min, versus 0.89% (Figure 3).

Membrane Integrity Assays. The diS-C_3(5) dye is widely used to monitor ion permeability and membrane potential in a variety of cells (*34*). This dye was used to monitor the transmembrane potential changes induced by plasticins on *S. aureus* ST1065. Results are reported in Figure 4A. Except for the neutral plasticin-DA1 (data not shown), all tested plasticins had similar effects on the polarization state of *S. aureus* ST1065 and led to

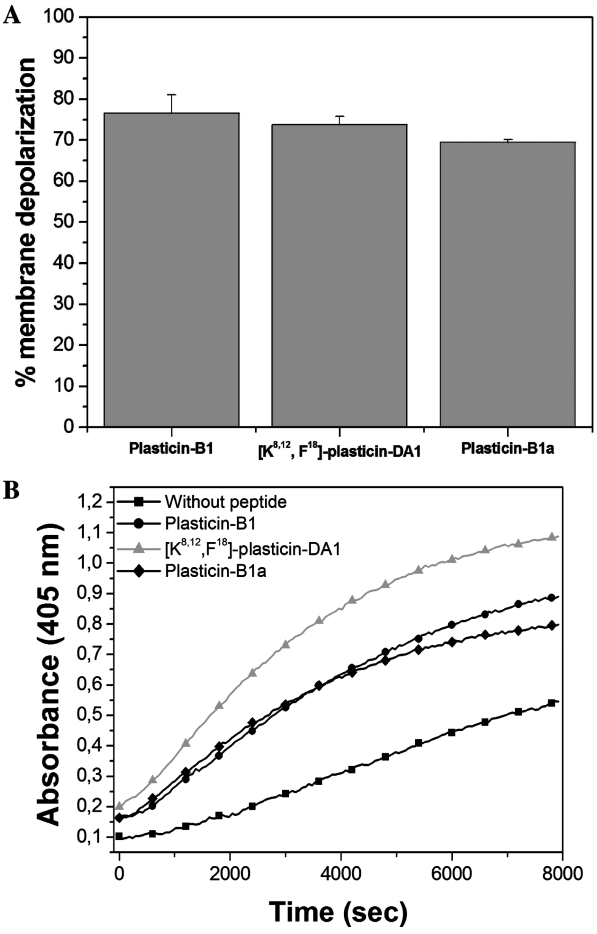

FIGURE 4: Membrane integrity assays using *S. aureus* strain ST1065. Quantification of the depolarization efficiency (%) (A) by measurement of the level of release of diS-$C_3(5)$ fluorescent probe relative to the Triton X-100 effect and (B) by permeabilization of the bacterial cytoplasmic membrane monitored by measuring β-galactosidase activity. For both results presented here, peptide concentrations were 10 μM.

a strong depolarization (approximately 75%) of this bacterial strain. Similar depolarization potencies were also found with *S. epidermidis* (Figure S1 of the Supporting Information). The permeabilization potentials of plasticin-B1, plasticin-B1a, and [$K^{8,12}$,F^{18}]plasticin-DA1 were evaluated on *S. aureus* ST1065 which has strong β-galactosidase production. As shown in Figure 4B, plasticins were permeabilizing the cytoplasmic membrane of *S. aureus* ST1065. [$K^{8,12}$, F^{18}]-plasticin-DA1 appears to be the more efficient while plasticin-B1 and plasticin-B1a have a similar permeabilization potential. Taken together, these results indicate that the bacterial cytoplasmic membrane is an important target for the selected plasticins.

Membrane Models for Biophysical Investigations. Lipids with phosphatidylglycerol (PG) headgroups are major components of bacterial cytoplasmic membranes. However, plasma membranes of CAMPs-resistant strains are depleted of anionic charges (*9*). Consequently, the anionic lipid DMPG was used to mimic the native *S. aureus* cytoplasmic membrane, while zwitterionic DMPC and a mixture of DMPG and DMPE (3:1) were used as membrane models to mimic negative charge-depleted membranes of CAMP-resistant strains.

Macroscopic Interfacial Organization of Plasticins. Monolayers and films constitute a useful platform for studying membrane-active peptides (*38*), particularly providing information

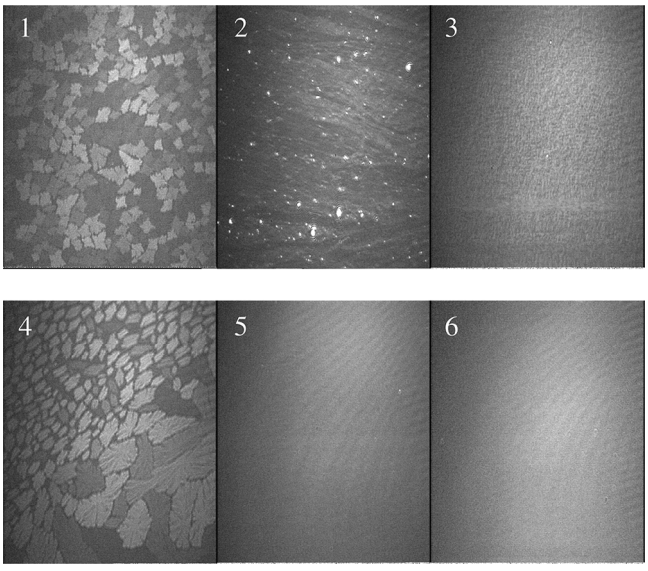

FIGURE 5: Interface behavior and perturbation of lipid macroscopic organization in plasticin-B1 and [$K^{8,12}$,F^{18}]plasticin-DA1. Images were recorded using BAM of the air−buffer interface (1 or 4), the DMPC monolayer−buffer interface (2 or 5), or the DMPG monolayer−buffer interface (3 or 6) in the presence of a plasticin (plasticin-B1 or [$K^{8,12}$,F^{18}]plasticin-DA1, respectively). Peptides were injected in the subphase. Images were 650 μm × 450 μm in size and recorded with a shutter speed of 50.

about peptide association and studying effects of lipid monolayers on peptide surface organization.

The morphology of the phospholipid monolayer was investigated by Brewster angle microscopy (BAM) at a constant lateral pressure of 25 mN/m for both DMPC and DMPG. BAM allows the direct observation of ultrathin films on air−water interfaces (e.g., a monolayer with a thickness of 2 nm). As shown in Figure 5, BAM images differ according to phospholipid species and peptides. With pure peptides, the air−buffer interface was constituted with little domains of different gray levels. BAM images are coded in gray levels, which can be calibrated in absolute reflectance. The calibration function is established by comparison between the experimental curve of the gray level and the theoretical Fresnel curve on the water surface. Thickness evaluation was achieved via the proportional relation between the reflectance of the film and the square of its interfacial thickness when its optical index is assumed to be constant. However, we suspect here that the different domains all have the same thickness but different birefringence angles that may be due to a specific orientation of the peptide in each domain. Moreover, [$K^{8,12}$,F^{18}]plasticin-DA1 forms domains with different sizes unlike plasticin B1 which forms very regular domains.

When plasticins were injected underneath the DMPC monolayer, bright spots were observed for plasticin-B1 but not for [$K^{8,12}$,F^{18}]plasticin-DA1 (Figure 5, panels 2 and 5). These bright spots underline plasticin-B1's propensity to form condensed domains during its interaction with the DMPC monolayer. This property was not observed for [$K^{8,12}$,F^{18}]plasticin-DA1 with DMPC (Figure 5, panel 5) or with DMPG monolayers with any of the tested peptides (Figure 5, panels 3 and 6).

During the BAM experiments, the lateral pressure was followed using the Wilhelmy method. With a DMPC monolayer, after injection of the peptide in the subphase, we observed a strong increase in the lateral pressure (Figure S2 of the Supporting Information), indicating that both plasticin-B1 and

Table 3: Structural Interconversions and Orientation of Plasticins at the Interface of DMPG and DMPC Monolayers[a]

interface		main conformations	amide I × 10^4	amide II × 10^4	ratio	orientation
air−buffer	plasticin-B1	α-helix	50.159	26.75	1.9	45°
	[$K^{8,12}$,F^{18}]plasticin-DA1	α-helix	24.935	0.51	48.9	flat
DMPG monolayer	plasticin-B1	α-helix/random coil/β-structures	40.897	8.36	4.9	practically flat
	[$K^{8,12}$,F^{18}]plasticin-DA1	α-helix/β-turn	31.31	2.56	12.2	flat
DMPC monolayer	plasticin-B1	α-helix	17.788	7.44	2.4	20°
	[$K^{8,12}$,F^{18}]plasticin-DA1	α-helix	38.434	3.62	10.6	flat

[a]Helix orientation compared to air−solvent and lipid−solvent interfaces is deduced from the amide I:amide II intensity ratios determined by PM-IRRAS spectra (Figure S3 of the Supporting Information) as previously described (*58*).

[$K^{8,12}$,F^{18}]plasticin-DA1 insert into this monolayer. With the DMPG monolayer, after injection, we saw a slight increase in the lateral pressure followed by a surface pressure decrease. Results underline that both peptides formed more packed lipid domains than the monolayer without peptide and that they did not insert into (or only partially) the DMPG monolayer. This phenomenon was not observed with the DMPC monolayer even if the injections were made with small volumes of the peptide solution (Figure S2 of the Supporting Information).

BAM also allows the estimation of the film thickness observed using gray level reflectivity. Without any films, the average gray level reflectivity was ~15.13×10^{-8}. After addition of plasticin-B1 and [$K^{8,12}$,F^{18}]plasticin-DA1, it increased to 95.27×10^{-8} and 101.12×10^{-8}, respectively. From these data, the thicknesses of the peptide film were determined to be approximately 12.5 and 13.6 Å, respectively. With a DMPC monolayer, the thicknesses were estimated to be 12.6 and 12 Å for plasticin-B1 and [$K^{8,12}$, F^{18}]plasticin-DA1, respectively. With the DMPG monolayer, the thickness was 14.5 Å for plasticin-B1 and 12.7 Å for [$K^{8,12}$, F^{18}]plasticin-DA1. The refractive index used is 1.47. These thicknesses are in good agreement with a flat or weakly tilted insertion of the peptide in an α-helix conformation in (DMPC) or under (DMPG) the monolayer (the diameter of an α-helix is approximately 12.5 Å).

Interfacial Conformation and Orientation of Plasticins. PM-IRRAS is a powerful technique for determining the in situ conformation and orientation of a peptide in ultrathin films at the air−water interface (*36*). PM-IRRAS was used here to investigate the structure and orientation of plasticin-B1 and [$K^{8,12}$,F^{18}]plasticin-DA1. The secondary structure of these plasticins can be estimated from the frequency position and intensity of the amide bands. Plasticins presented a major amide I band centered at 1656 cm^{-1} under all the tested conditions (Figure S3 of the Supporting Information), showing that plasticins were mainly structured in α-helices at interfaces (air−buffer or phospholipid−buffer interfaces) (Table 3). Nevertheless, the spectrum of [$K^{8,12}$,F^{18}]plasticin-DA1 displayed a band at 1680 cm^{-1} that corresponds to a β-turn structure indicating that the peptide was not a pure helix. Moreover, the amide I band of plasticin-B1 with the DMPG monolayer showed an expansion at its base corresponding to a significant proportion of random coil and/or β-sheet in the structure of this peptide while interacting with the anionic monolayer.

At the air−buffer interface, the amide I:amide II intensity ratio was ~1.9 for plasticin-B1, indicating that this peptide was tilted at a 45° angle compared to the interface (Table 3). On the other hand, the [$K^{8,12}$,F^{18}]plasticin-DA1 helix was flat at the air−buffer interface as demonstrated by its amide I:amide II intensity ratio of 4.9. At the phospholipid−buffer interface, plasticins mainly had a flat orientation except plasticin-B1 that was slightly angled at 20° with respect to the interface. We note that [$K^{8,12}$,F^{18}]plasticin-DA1 first inserts into the monolayer as an α-helix oriented at approximately 30° compared to the interface (data not shown) and then adopts a flat helix orientation after equilibrium had been maintained for a few minutes, contrasting with plasticin-B1 which displays a quasi-instantaneous reorganization at the membrane interface.

Effects of Plasticins on Phospholipid Monolayers. The PM-IRRAS technique also allows the evaluation of perturbation of phospholipid structure or orientation, using the ν(C=O) band centered around 1730 cm^{-1}. Taking into account this band and the $\delta(CH_2)$ band centered around 1450 cm^{-1}, we showed that plasticin-B1 strongly disturbed the DMPC monolayer by provoking phospholipid reorganization (phospholipids adopt a more vertical position compared to the interface) (data not shown). This movement was less important with the DMPG monolayer and was not observed with [$K^{8,12}$, F^{18}]plasticin-DA1.

Effects of Plasticins on Lipid-Phase Transitions As Assessed by DSC. DSC is a powerful tool for studies of lipid−protein interactions with model and biological membranes, and there is a growing interest in this approach within the area of membranotropic peptides such as AMPs (*39*). Various MLV lipid-containing systems were used to study the effects of plasticins on the thermotropic-phase behavior of the selected phospholipids. A relatively large range of peptide:lipid ratios was studied, allowing us to explore the different steps of membrane binding and disruption as detailed below. Detailed thermogram analysis at a peptide:lipid ratio of 1:20 is provided in Table S2 of the Supporting Information.

Anionic Staphylococcal Mimetic Membrane (*DMPG*). DSC endotherms illustrating the effect of plasticins on the thermotropic phase of DMPG MLVs at different lipid:peptide ratios are presented in Figure 6. The thermogram of MLVs without addition of peptide showed a weakly energetic transition around 12 °C and a higher energetic transition around 23 °C. The pretransition was gradually abolished when the peptide:lipid ratio was increased, for any of the tested plasticins, while multiple effects on the main transition could be noticed. Three behaviors were observed: (i) plasticin-B1 and its carboxamidated version behaved similarly with a substantial decrease in the cooperativity of the main transition accompanied by the presence of slightly higher temperature transitions, usually assigned to peptide-poor domain formation; (ii) [$K^{8,12}$,F^{18}]plasticin-DA1 presented a complex melting profile that could be decomposed into at least two components, one corresponding to the pure lipid phase and

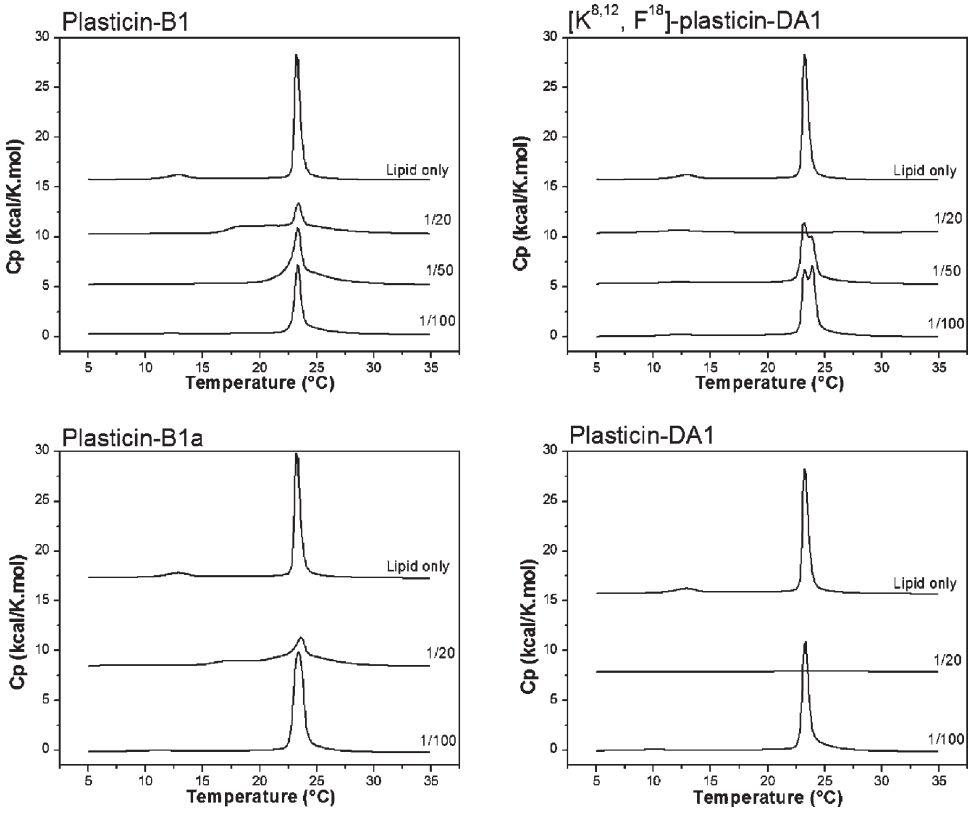

FIGURE 6: Peptide membrane perturbation using an anionic staphylococcal mimetic membrane. DSC heating scans illustrating the effect of selected plasticins at various peptide:lipid ratios on the thermotropic-phase behavior of DMPG. Thermograms of pure lipids are also presented for the sake of comparison. Data on the neutral plasticin-DA1 are also presented here to probe the effect of peptide charge on lipid-phase organization.

a second shoulder at higher transition temperatures that might correspond to lipid domains with a stabilized gel phase due to interactions with peptides; and (iii) plasticin-DA1 slightly decreased the enthalpy of the main transition and totally abolished it at a 1:20 peptide:lipid ratio, indicating total disorganization of the lipid DMPG bilayer.

Negative Charge-Depleted Membrane Models (*DMPC and DMPG/DMPE*). DSC endotherms illustrating the effect of plasticins on the thermotropic phase of DMPC MLVs at different lipid:peptide ratios are presented in Figure 7. The thermogram of MLVs without the addition of peptides showed a weakly energetic transition around 13 °C and a higher energetic transition around 24 °C. For most experiments, the cooling exotherms of DMPC in interaction with the selected plasticins exhibited near-mirror images relative to the heating endotherms (data not shown), indicating that the major thermotropic events were recorded under conditions very close to thermodynamic equilibrium. The pretransition was gradually abolished for all plasticins except plasticin-DA1 when the peptide:lipid ratio was increased, while multiple effects on the main transition were observed (Figure 7 and Table S2 of the Supporting Information). A small effect on the temperature transition was observed for all plasticins except for [$K^{8,12}$,F^{18}]plasticin-DA1, showing a noticeable increase in this temperature (1 °C). The relative perturbation of the thermotropic-phase behavior increased in the following order: [$K^{8,12}$,F^{18}]plasticin-DA1≫ plasticin-DA1 > plasticin-B1 ≈ plasticin-B1a.

DSC endotherms illustrating the effects of plasticins on the thermotropic phase of DMPG/DMPE (3:1) MLVs mimicking partial anionic charge-depleted membranes of resistant strains at different lipid:peptide ratios are presented in Figure S4 of the Supporting Information. The thermogram of the pure lipid mixture showed a single transition near 44 °C, attributed to the Lβ−Lα phase transition. The relative perturbation of the thermotropic-phase behavior, although modest, increased in the following order: plasticin-DA1 > plasticin-B1a > plasticin-B1 ≈ [$K^{8,12}$,F^{18}]plasticin-DA1. In all cases, no lipid segregation was observed. Overall, the plasticins induced a smaller reorganization of the DMPG/DMPE MLV lipid assembly than of DMPG or DMPC.

DISCUSSION

In this study, we have conducted an in-depth comparative analysis of the staphylococcidal efficiency and interfacial properties of two closely related plasticins, plasticin-B1 and [$K^{8,12}$, F^{18}]plasticin-DA1, that bear the same net charge (+2). Our findings are summarized in Table 4.

Immunostimulatory Potential of Investigated Plasticins. Many AMPs have multiple effects on the immune response and thus operate as essential multifunctional endogenous effectors of host innate defense against invasion by pathogenic microorganisms. One of the primary defense barriers against *S. aureus* infection is the innate immunity provided by neutrophils (*15*). Thus, topical applications of AMPs that also display immunostimulatory activity are highly desirable in combating staphylococcal infections. Only a few studies dealing with neutrophil chemoattractive activities of frog skin AMPs have been reported in the literature. Demonstrated chemotaxis was related to amphipathic α-helical peptides such as Drs-S1 (*40*), temporin A and analogues (*41*), and recently a β-structured peptide, Drs-S9 (*14*). Plasticin B1 was shown to induce chemotaxis in the same

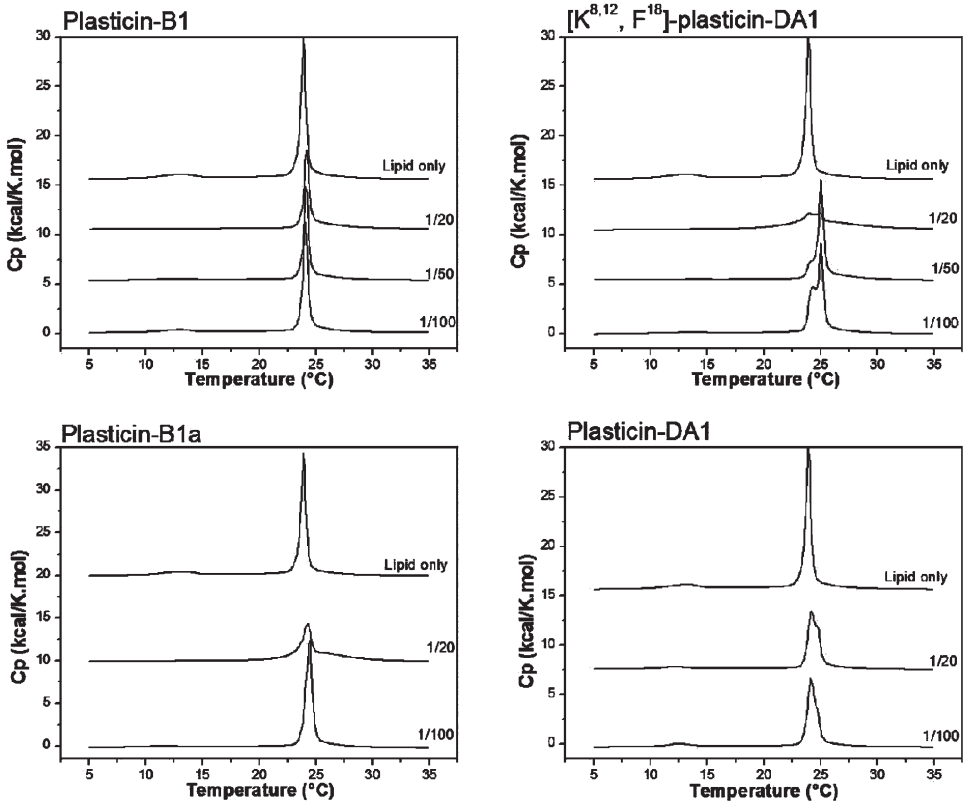

FIGURE 7: Peptide membrane perturbation effect on a negative charge-depleted membrane model mimicking membranes of the cationic AMP-resistant strain. DSC heating scans illustrating the effect of selected plasticins on the thermotropic-phase behavior of a negative charge-depleted membrane model (DMPC). Thermograms of pure lipids are also presented for the sake of comparison.

Table 4: Main Features of [$K^{8,12}$,F^{18}]Plasticin-DA1 versus Plasticin-B1

	[$K^{8,12}$,F^{18}]plasticin-DA1	plasticin-B1
Efficiency against MRSA	−	+
Sensitivity of a Δ*graSR* mutant	prolonged lag phase	−
Maximum chemotactic response	1 μM	10 nM
Permeabilization of the *Staphylococcus* cytoplasmic membrane	+ +	+
Interfacial activity	formation of irregular domains	formation of regular domains
Structure and orientation at the membrane interface	β-turn/α-helix flat α-helix after a slow reorientation	flexible α-helix
Effects on lipid transition phases	complex main transition[a] peptide-poor and peptide-rich domains[a]	interaction with headgroups[a]

[a]Anionic membrane model. Negative charge-depleted membrane model.

range of concentrations as Drs-S1 (10 nM) or temporin A (250 nM), whereas [$K^{8,12}$,F^{18}]plasticin-DA1 was efficient at micromolar concentrations. Chemotactic receptors are very sensitive to ligand concentrations. For example, the formyl peptide receptor (FPR) is defined as a high-affinity receptor and is activated by picomolar to low nanomolar concentrations of ligand, whereas formyl peptide receptor-like 1 (FPRL-1) is defined as a low-affinity receptor that binds the ligand at high concentrations (~100 nM). Thus, our results suggest that plasticins could be recognized by at least two different receptors, a high-affinity receptor and a low-affinity receptor, for plasticin B1 and [$K^{8,12}$, F^{18}]plasticin-DA1, respectively. It is also noteworthy that an interesting correlation was observed between the ability of the peptides to inhibit growth of *S. aureus* MRSA strains and chemotactic potency: [$K^{8,12}$,F^{18}]plasticin-DA1, found to be inactive against the MRSA strains, induced chemotaxis only at concentrations 100-fold higher than those of plasticin-B1 (Figure 1).

Relationship among Membrane Disturbing Activity, Susceptibility of the GrasS/GraR Two-Component System, and Bactericidal Activity. Understanding the specificity and mode of action of existing bacterial peptide resistance mechanisms is essential in addressing the problem of drug resistance development. The main CAMP resistance mechanism described in *S. aureus* involves the GrasS/GraR two-component system. Growth of *S. aureus* RN1 HG and ST1036 (Δ*graRS* in the presence of plasticins) revealed a stronger antimicrobial effect of plasticin-B1a and [$K^{8,12}$,F^{18}]plasticin-DA1 against the TCS-lacking strain, while no difference was detected when plasticin-B1 was added to the culture. It has been suggested that the GraS/GraR TCS is only activated by positively charged AMPs, but the response intensity has not been directly correlated with the amount of positive charge or secondary peptide structure. However, we have shown here that plasticin-B1a, a peptide with a net charge of +3, is more efficient against the parental strain and the Δ*graRS* mutant than [$K^{8,12}$,F^{18}]plasticin-DA1 with a net

charge of +2 (Figure 2). In bactericidal assays, plasticin-B1a was 40-fold more active than [$K^{8,12}$,F^{18}]plasticin-DA1 against the wild-type RN1 HG strain. Nevertheless, plasticin-B1 (net charge of +2) had no effect on the growth of the two strains under our conditions, indicating that modifications such as amidation and secondary structure differences may play a key role in peptide sensing at the bacterial surface. A recent comparative study of peptide bactericidal activities (temporins and esculentins from *Rana* and bombinins from *Bombina*) showed that, as for plasticins, a high positive charge is not an absolute requirement for bactericidal activity against MRSA strains but that charge distribution along the helix and hydrophobicity seem to be critical elements (*12*). Another possible effect of amidation is to protect peptides against the action of proteases (*42*). Peptide stability is thus enhanced, and this could play a role in the higher activity of amidated plasticins, as found for magainin 2 analogues (*43*). Many studies indicate that antibacterial peptide inactivation through proteolysis is widespread among pathogenic bacteria (*44*). In particular, bactericidal activity of human unamidated cathelicidin LL37 is inactivated by aureolysin, a metalloprotease from *S. aureus* (*45*), and staphylokinase, produced by the strains studied here, is also known to cleave certain CAMPs (*46*).

Further work is needed to determine whether the degree of positive charges, their accessibility, and peptide stability are the only factors involved in the differential GraSR-dependent response. We showed that the Δ*graRS* mutant is able to grow in the presence of high [$K^{8,12}$,F^{18}]plasticin-DA1 concentrations only after a 10−13 h lag. The reason for this late resistance could involve the induction of a secondary resistance system, specific peptidase production, or cell wall modifications and will be the subject of further study.

Because of their high degree of similarity, the two investigated plasticins may cross similarly the LTA layer to reach the cytoplasmic negatively charged target membrane. Additionally, membrane integrity assays clearly demonstrated that plasticins target the *S. aureus* cytoplasmic membrane (Figure 4). Interestingly, although [$K^{8,12}$,F^{18}]plasticin-DA1 had lower staphylocidal activity, it efficiently disturbs the membrane potential and affects the membrane permeability of *S. aureus* ST1065. This suggests that the capacity to modify some membrane characteristics is not sufficient for determining peptide bacterial killing potency (*47*, *48*).

Membrane Effects and Interfacial Behavior. It is well-known that the net charge of the *S. aureus* cell envelope affects the susceptibility toward AMPs (*9*). For example, MprF-dependent lysinylation of PG, constituting 80% of the phospholipids, contributes to the relative positive charge of the *S. aureus* cell surface and correlates with in vitro resistance to a number of CAMPs (*9*). Additionally, DltA-dependent D-alanylation of teichoic acids also increases the net positive charge of the *S. aureus* cell surface (*49*). Hence, it has been suggested that electrostatic repulsion may be crucial in CAMP resistance. Perturbation of the *S. aureus* cytoplasmic membrane is believed to play an important role in bactericidal mechanisms for many AMPs (*47*). Through the use of microcalorimetry (DSC) together with PM-IRRAS and BAM on various membrane models mimicking the cytoplasmic membrane of wild-type and CAMP-resistant strains of *S. aureus*, we were able to establish a relationship among staphylococcidal efficiency, bacterial resistance, and peptide−membrane interactions. Membrane permeabilization thus appears to be dependent on a peptide having the correct balance of hydrophobicity, solubility, amphipathicity, and propensity to self-assemble on membranes into peptide-rich domains.

We were thus able to elucidate multiple mechanisms of membrane disruption by [$K^{8,12}$,F^{18}]plasticin-DA1 and plasticin-B1. DSC information supports the notion that peptides affect lipid packing in membranes, as evidenced by the formation of both peptide-rich and peptide-poor domains (Table 4). Furthermore, one can notice similar effects on lipid-phase transitions on DMPG MLVs observed with the neutral plasticin-DA1 and plasticin-B1a (charges of +3), again indicating that peptide charge is not the only factor in peptide efficiency (Figure 6). Peptides and proteins interacting with the hydrophobic core region of the membranes often exhibit a large reduction in transition enthalpy (*50*, *51*). Furthermore, the progression of the main transition complexity is consistent with the separation of the lipid surface into peptide or peptide-deficient domains. We have also showed that [$K^{8,12}$,F^{18}]plasticin-DA1 autoassociates in the presence of PG (*21*), a major component of the *S. aureus* bacterial cell membrane, which may in part explain the selectivity in antimicrobial activity of this peptide toward *E. coli* versus *S. aureus*. Epand and collaborators have recently made a systematic comparison between antimicrobial efficiencies against a large panel of bacterial strains and lipid domain formation observed by DSC. They suggest that antibacterial selectivity among AMPs may come from clustering of anionic lipids and their segregation into domains (*52*).

These differential effects on lipids can be connected to the orientation of plasticins with respect to lipid monolayers deduced from PM-IRRAS analysis. As shown in Table 3, plasticin-B1 and [$K^{8,12}$,F^{18}]plasticin-DA1 differ in their structural interconversion behavior as well as in their kinetics of reorganization at the membrane interface composed of both DMPG and DMPC lipids.

The two investigated plasticins were shown to bind tightly to negatively charged or mixed membrane mimetic systems; the peptides initially reside, if not at the surface, then in the interface region. Plasticins nearly span the membrane and thus could form channels, and their antimicrobial activity could arise from the ability to alter membrane characteristics and/or cross the membrane spontaneously and act on intracellular targets or perturb the coordination of multienzymatic complexes located in the vicinity of the membrane (*53*). In addition to amphipathicity and cationicity, plasticity of molecular interactions between membranotropic peptides and biomembranes is increasingly being acknowledged as a factor that may allow a better understanding of antimicrobial peptide mechanisms of action. Structural polymorphism may be crucial since it provides peptides with the possibility of adapting their conformation to medium hydrophobicity and/or to partner diversity (*54*).

Our early assumption was that the β-hairpin-shaped conformation for [$K^{8,12}$,F^{18}]plasticin-DA1 preformed in solution may act as a conformational lock preventing the switch to α-helical structure, thus lowering antimicrobial effectiveness (*18*). Here, thanks to PM-IRRAS experiments, we have been able to monitor and quantify in situ structural interconversions and peptide orientations at the membrane interface and expand our previous findings from FTIR transmission spectroscopy. Previous conformational studies on plasticins had concluded that plasticin-B1a formed a rather rigid α-helix while plasticin-B1 displayed a more flexible one (*18*, *19*). This is in accordance with the fact that activity against the Gram-positive pathogen *S. aureus* was primarily observed for peptides associating a relatively high net

charge and a propensity to adopt a well-defined α-helical conformation with an amphipathic character. However, as reported by Rathinakumar et al. (*22*), and suggested in this work, secondary structure and biological activity are poorly coupled, consistent with the hypothesis that AMPs do not form pores of well-defined structure in membranes but rather destabilize membranes by partitioning into membrane interfaces and disturbing the organization of the lipids, a property they designate "interfacial activity".

CONCLUSION

Our data also bring new data to the physicochemical parameters determining the sensitivity of the GraS/GraR two-component system to CAMPs. We address here the fact that structural interconversions at the membrane interface of the representative plasticins rather than their secondary structures give clues explaining the differential susceptibilities. Moreover, peptide charge seemed not to be a determinant for explaining the observed staphyloccocidal potencies; rather, charge distribution might be more relevant. Additional data are needed to determine whether the degree of positive charges, their accessibility, and peptide stability are the only factors involved in the differential GraSR-dependent response. Membrane models, although minimalist, allowed us to point out features that can be linked to staphylococcidal efficacy. We also provide a quantitative in situ picture of interfacial behaviors and underline the fact that the kinetics of conformational reorganization differs markedly between the investigated plasticins.

ACKNOWLEDGMENT

We thank Silvia Herbert and Friedrich Götz for providing us with *S. aureus* strain RN1 HG. We thank Dr. Christophe Piesse from the "Ingénierie des protéines et synthèse peptidique" plateforme of the Institut de Biologie intégrative, IFR 83, for the synthesis of plasticin analogues. We are also grateful to Isabel Alves (CNRS, UMR 7613 of UPMC) and Jennifer Bourgeois and Julien Nicolas (CNRS, UMR 8612, Université Paris-Sud XI) for MLV and LUV preparation facilities and helpful discussions.

SUPPORTING INFORMATION AVAILABLE

Additional data on bactericidal potencies (multiresistant non *aureus* strains), membrane disturbing properties (DSC and depolarization efficiency), and interfacial behavior (PM-IRRAS spectra and measurement of the variation of monolayer surface area). This material is available free of charge via the Internet at http://pubs.acs.org.

REFERENCES

1. Nicolas, P., and Mor, A. (1995) Peptides as weapons against microorganisms in the chemical defense system of vertebrates. *Annu. Rev. Microbiol. 49*, 277–304.
2. Zasloff, M. (2002) Antimicrobial peptides of multicellular organisms. *Nature 415*, 389–395.
3. Nicolas, P., and El Amri, C. (2009) The dermaseptin superfamily: A gene-based combinatorial library of antimicrobial peptides. *Biochim. Biophys. Acta 1788*, 1537–1550.
4. Shai, Y. (1999) Mechanism of the binding, insertion and destabilization of phospholipid bilayer membranes by α-helical antimicrobial and cell non-selective membrane-lytic peptides. *Biochim. Biophys. Acta 1462*, 55–70.
5. Hancock, R. E., and Rozek, A. (2002) Role of membranes in the activities of antimicrobial cationic peptides. *FEMS Microbiol. Lett. 206*, 143–149.
6. Baba, T., Takeuchi, F., Kuroda, M., Yuzawa, H., Aoki, K., Oguchi, A., Nagai, Y., Iwama, N., Asano, K., Naimi, T., Kuroda, H., Cui, L., Yamamoto, K., and Hiramatsu, K. (2002) Genome and virulence determinants of high virulence community-acquired MRSA. *Lancet 359*, 1819–1827.
7. Gill, S. R., Fouts, D. E., Archer, G. L., Mongodin, E. F., Deboy, R. T., Ravel, J., Paulsen, I. T., Kolonay, J. F., Brinkac, L., Beanan, M., Dodson, R. J., Daugherty, S. C., Madupu, R., Angiuoli, S. V., Durkin, A. S., Haft, D. H., Vamathevan, J., Khouri, H., Utterback, T., Lee, C., Dimitrov, G., Jiang, L., Qin, H., Weidman, J., Tran, K., Kang, K., Hance, I. R., Nelson, K. E., and Fraser, C. M. (2005) Insights on evolution of virulence and resistance from the complete genome analysis of an early methicillin-resistant *Staphylococcus aureus* strain and a biofilm-producing methicillin-resistant *Staphylococcus epidermidis* strain. *J. Bacteriol. 187*, 2426–2438.
8. Giacometti, A., Cirioni, O., Barchiesi, F., and Scalise, G. (2000) In-vitro activity and killing effect of polycationic peptides on methicillin-resistant *Staphylococcus aureus* and interactions with clinically used antibiotics. *Diagn. Microbiol. Infect. Dis. 38*, 115–118.
9. Peschel, A. (2002) How do bacteria resist human antimicrobial peptides? *Trends Microbiol. 10*, 179–186.
10. Herbert, S., Bera, A., Nerz, C., Kraus, D., Peschel, A., Goerke, C., Meehl, M., Cheung, A., and Gotz, F. (2007) Molecular basis of resistance to muramidase and cationic antimicrobial peptide activity of lysozyme in staphylococci. *PLoS Pathog. 3*, e102.
11. Li, M., Cha, D. J., Lai, Y., Villaruz, A. E., Sturdevant, D. E., and Otto, M. (2007) The antimicrobial peptide-sensing system aps of *Staphylococcus aureus*. *Mol. Microbiol. 66*, 1136–1147.
12. Mangoni, M. L., Maisetta, G., Di Luca, M., Gaddi, L. M., Esin, S., Florio, W., Brancatisano, F. L., Barra, D., Campa, M., and Batoni, G. (2008) Comparative analysis of the bactericidal activities of amphibian peptide analogues against multidrug-resistant nosocomial bacterial strains. *Antimicrob. Agents Chemother. 52*, 85–91.
13. Mookherjee, N., and Hancock, R. E. (2007) Cationic host defence peptides: Innate immune regulatory peptides as a novel approach for treating infections. *Cell. Mol. Life Sci. 64*, 922–933.
14. Auvynet, C., El Amri, C., Lacombe, C., Bruston, F., Bourdais, J., Nicolas, P., and Rosenstein, Y. (2008) Structural requirements for antimicrobial versus chemoattractant activities for dermaseptin S9. *FEBS J. 275*, 4134–4151.
15. Foster, T. J. (2005) Immune evasion by staphylococci. *Nat. Rev. Microbiol. 3*, 948–958.
16. Marr, A. K., Gooderham, W. J., and Hancock, R. E. (2006) Antibacterial peptides for therapeutic use: Obstacles and realistic outlook. *Curr. Opin. Pharmacol. 6*, 468–472.
17. El Amri, C., and Nicolas, P. (2008) Plasticins: Membrane-damaging peptides with 'chameleon-like' properties. *Cell. Mol. Life Sci. 65*, 895–909.
18. Bruston, F., Lacombe, C., Zimmermann, K., Piesse, C., Nicolas, P., and El Amri, C. (2007) Structural malleability of plasticins: Preorganized conformations in solution and relevance for antimicrobial activity. *Biopolymers 86*, 42–56.
19. El Amri, C., Lacombe, C., Zimmerman, K., Ladram, A., Amiche, M., Nicolas, P., and Bruston, F. (2006) The plasticins: Membrane adsorption, lipid disorders, and biological activity. *Biochemistry 45*, 14285–14297.
20. Vanhoye, D., Bruston, F., El Amri, S., Ladram, A., Amiche, M., and Nicolas, P. (2004) Membrane association, electrostatic sequestration, and cytotoxicity of Gly-Leu-rich peptide orthologs with differing functions. *Biochemistry 43*, 8391–8409.
21. Joanne, P., Galanth, C., Goasdoue, N., Nicolas, P., Sagan, S., Lavielle, S., Chassaing, G., El Amri, C., and Alves, I. D. (2009) Lipid reorganization induced by membrane-active peptides probed using differential scanning calorimetry. *Biochim. Biophys. Acta 1788*, 1772–1781.
22. Rathinakumar, R., Walkenhorst, W. F., and Wimley, W. C. (2009) Broad-Spectrum Antimicrobial Peptides by Rational Combinatorial Design and High-Throughput Screening: The Importance of Interfacial Activity. *J. Am. Chem. Soc. 131*, 7609–7617.
23. Rathinakumar, R., and Wimley, W. C. (2008) Biomolecular engineering by combinatorial design and high-throughput screening: Small, soluble peptides that permeabilize membranes. *J. Am. Chem. Soc. 130*, 9849–9858.
24. Arnaud, M., Chastanet, A., and Debarbouille, M. (2004) New vector for efficient allelic replacement in naturally nontransformable, low-GC-content, Gram-positive bacteria. *Appl. Environ. Microbiol. 70*, 6887–6891.
25. Agaisse, H., and Lereclus, D. (1994) Structural and functional analysis of the promoter region involved in full expression of the

cryIIIA toxin gene of *Bacillus thuringiensis*. *Mol. Microbiol. 13*, 97–107.
26. Sullivan, M. A., Yasbin, R. E., and Young, F. E. (1984) New shuttle vectors for *Bacillus subtilis* and *Escherichia coli* which allow rapid detection of inserted fragments. *Gene 29*, 21–26.
27. Zuber, P., and Losick, R. (1983) Use of a lacZ fusion to study the role of the spoO genes of *Bacillus subtilis* in developmental regulation. *Cell 35*, 275–283.
28. Perkins, J. B., and Youngman, P. J. (1986) Construction and properties of Tn917-lac, a transposon derivative that mediates transcriptional gene fusions in *Bacillus subtilis*. *Proc. Natl. Acad. Sci. U.S.A. 83*, 140–144.
29. Biswas, R., Voggu, L., Simon, U. K., Hentschel, P., Thumm, G., and Gotz, F. (2006) Activity of the major staphylococcal autolysin Atl. *FEMS Microbiol. Lett. 259*, 260–268.
30. Boyum, A. (1968) Isolation of leucocytes from human blood. Further observations. Methylcellulose, dextran, and ficoll as erythrocyteaggregating agents. *Scand. J. Clin. Lab. Invest., Suppl. 97*, 31–50.
31. Deng, X., Ueda, H., Su, S. B., Gong, W., Dunlop, N. M., Gao, J. L., Murphy, P. M., and Wang, J. M. (1999) A synthetic peptide derived from human immunodeficiency virus type 1 gp120 downregulates the expression and function of chemokine receptors CCR5 and CXCR4 in monocytes by activating the 7-transmembrane G-protein-coupled receptor FPRL1/LXA4R. *Blood 94*, 1165–1173.
32. Chesneau, O., Ligeret, H., Hosan-Aghaie, N., Morvan, A., and Dassa, E. (2005) Molecular analysis of resistance to streptogramin A compounds conferred by the Vga proteins of staphylococci. *Antimicrob. Agents Chemother. 49*, 973–980.
33. Sims, P. J., Waggoner, A. S., Wang, C. H., and Hoffman, J. F. (1974) Studies on the mechanism by which cyanine dyes measure membrane potential in red blood cells and phosphatidylcholine vesicles. *Biochemistry 13*, 3315–3330.
34. Suzuki, H., Wang, Z. Y., Yamakoshi, M., Kobayashi, M., and Nozawa, T. (2003) Probing the transmembrane potential of bacterial cells by voltage-sensitive dyes. *Anal. Sci. 19*, 1239–1242.
35. Henon, S., and Meunier, J. (1991) Microscope at the Brewster angle: Direct observation of first-order phase transitions in monolayers. *Rev. Sci. Instrum. 62*, 936–939.
36. Blaudez, D., Turlet, J. M., Dufourcq, J., Bard, D., Buffeteau, T., and Desbat, B. (1996) Investigations at the air/water interface using polarization modulation infrared spectroscopy. *J. Chem. Soc., Faraday Trans. 92*, 525–530.
37. Trad, S., Allignet, J., Frangeul, L., Davi, M., Vergassola, M., Couve, E., Morvan, A., Kechrid, A., Buchrieser, C., Glaser, P., and El-Solh, N. (2004) DNA macroarray for identification and typing of *Staphylococcus aureus* isolates. *J. Clin. Microbiol. 42*, 2054–2064.
38. Volinsky, R., Kolusheva, S., Berman, A., and Jelinek, R. (2006) Investigations of antimicrobial peptides in planar film systems. *Biochim. Biophys. Acta 1758*, 1393–1407.
39. Andrushchenko, V. V., Vogel, H. J., and Prenner, E. J. (2007) Interactions of tryptophan-rich cathelicidin antimicrobial peptides with model membranes studied by differential scanning calorimetry. *Biochim. Biophys. Acta 1768*, 2447–2458.
40. Ammar, B., Perianin, A., Mor, A., Sarfati, G., Tissot, M., Nicolas, P., Giroud, J. P., and Roch-Arveiller, M. (1998) Dermaseptin, a peptide antibiotic, stimulates microbicidal activities of polymorphonuclear leukocytes. *Biochem. Biophys. Res. Commun. 247*, 870–875.
41. Chen, Q., Wade, D., Kurosaka, K., Wang, Z. Y., Oppenheim, J. J., and Yang, D. (2004) Temporin A and related frog antimicrobial peptides use formyl peptide receptor-like 1 as a receptor to chemoattract phagocytes. *J. Immunol. 173*, 2652–2659.
42. Walker, J. R., Altman, R. K., Warren, J. W., and Altman, E. (2003) Using protein-based motifs to stabilize peptides. *J. Pept. Res. 62*, 214–226.
43. Juretic, D., Chen, H. C., Brown, J. H., Morell, J. L., Hendler, R. W., and Westerhoff, H. V. (1989) Magainin 2 amide and analogues. Antimicrobial activity, membrane depolarization and susceptibility to proteolysis. *FEBS Lett. 249*, 219–223.
44. Braff, M. H., Jones, A. L., Skerrett, S. J., and Rubens, C. E. (2007) *Staphylococcus aureus* exploits cathelicidin antimicrobial peptides produced during early pneumonia to promote staphylokinase-dependent fibrinolysis. *J. Infect. Dis. 195*, 1365–1372.
45. Sieprawska-Lupa, M., Mydel, P., Krawczyk, K., Wojcik, K., Puklo, M., Lupa, B., Suder, P., Silberring, J., Reed, M., Pohl, J., Shafer, W., McAleese, F., Foster, T., Travis, J., and Potempa, J. (2004) Degradation of human antimicrobial peptide LL-37 by *Staphylococcus aureus*-derived proteinases. *Antimicrob. Agents Chemother. 48*, 4673–4679.
46. Jin, T., Bokarewa, M., Foster, T., Mitchell, J., Higgins, J., and Tarkowski, A. (2004) *Staphylococcus aureus* resists human defensins by production of staphylokinase, a novel bacterial evasion mechanism. *J. Immunol. 172*, 1169–1176.
47. Koo, S. P., Bayer, A. S., and Yeaman, M. R. (2001) Diversity in antistaphylococcal mechanisms among membrane-targeting antimicrobial peptides. *Infect. Immun. 69*, 4916–4922.
48. Xiong, Y. Q., Mukhopadhyay, K., Yeaman, M. R., Adler-Moore, J., and Bayer, A. S. (2005) Functional interrelationships between cell membrane and cell wall in antimicrobial peptide-mediated killing of *Staphylococcus aureus*. *Antimicrob. Agents Chemother. 49*, 3114–3121.
49. Weidenmaier, C., Peschel, A., Kempf, V. A., Lucindo, N., Yeaman, M. R., and Bayer, A. S. (2005) DltABCD- and MprF-mediated cell envelope modifications of *Staphylococcus aureus* confer resistance to platelet microbicidal proteins and contribute to virulence in a rabbit endocarditis model. *Infect. Immun. 73*, 8033–8038.
50. Lewis, R. N., Mannock, D. A., and McElhaney, R. N. (2007) Differential scanning calorimetry in the study of lipid phase transitions in model and biological membranes: Practical considerations. *Methods Mol. Biol. 400*, 171–195.
51. Andrushchenko, V. V., Aarabi, M. H., Nguyen, L. T., Prenner, E. J., and Vogel, H. J. (2008) Thermodynamics of the interactions of tryptophan-rich cathelicidin antimicrobial peptides with model and natural membranes. *Biochim. Biophys. Acta 1778*, 1004–1014.
52. Epand, R. M., and Epand, R. F. (2008) Lipid domains in bacterial membranes and the action of antimicrobial agents. *Biochim. Biophys. Acta 1788*, 289–294.
53. Pag, U., Oedenkoven, M., Sass, V., Shai, Y., Shamova, O., Antcheva, N., Tossi, A., and Sahl, H. G. (2008) Analysis of in vitro activities and modes of action of synthetic antimicrobial peptides derived from an α-helical 'sequence template'. *J. Antimicrob. Chemother. 61*, 341–352.
54. Deshayes, S., Decaffmeyer, M., Brasseur, R., and Thomas, A. (2008) Structural polymorphism of two CPP: An important parameter of activity. *Biochim. Biophys. Acta 1778*, 1197–1205.
55. Amiche, M., Ladram, A., and Nicolas, P. (2008) A consistent nomenclature of antimicrobial peptides isolated from frogs of the subfamily Phyllomedusinae. *Peptides 29*, 2074–2082.
56. Bayer, A. S., Kupferwasser, L. I., Brown, M. H., Skurray, R. A., Grkovic, S., Jones, T., Mukhopadhay, K., and Yeaman, M. R. (2006) Low-level resistance of *Staphylococcus aureus* to thrombin-induced platelet microbicidal protein 1 in vitro associated with qacA gene carriage is independent of multidrug efflux pump activity. *Antimicrob. Agents Chemother. 50*, 2448–2454.
57. Kuroda, M., Ohta, T., Uchiyama, I., Baba, T., Yuzawa, H., Kobayashi, I., Cui, L., Oguchi, A., Aoki, K., Nagai, Y., Lian, J., Ito, T., Kanamori, M., Matsumaru, H., Maruyama, A., Murakami, H., Hosoyama, A., Mizutani-Ui, Y., Takahashi, N. K., Sawano, T., Inoue, R., Kaito, C., Sekimizu, K., Hirakawa, H., Kuhara, S., Goto, S., Yabuzaki, J., Kanehisa, M., Yamashita, A., Oshima, K., Furuya, K., Yoshino, C., Shiba, T., Hattori, M., Ogasawara, N., Hayashi, H., and Hiramatsu, K. (2001) Whole genome sequencing of meticillin-resistant *Staphylococcus aureus*. *Lancet 357*, 1225–1240.
58. Cornut, I., Desbat, B., Turlet, J. M., and Dufourcq, J. (1996) In situ study by polarization modulated Fourier transform infrared spectroscopy of the structure and orientation of lipids and amphipathic peptides at the air-water interface. *Biophys. J. 70*, 305–312.